Ocean Engineering 175 (2019) 122–137

Contents lists available at ScienceDirect

Ocean Engineering

journal homepage: www.elsevier.com/locate/oceaneng

An investigation into the effect of biofouling on the ship hydrodynamic characteristics using CFD

Soonseok Song*, Yigit Kemal Demirel, Mehmet Atlar

Department of Naval Architecture, Ocean and Marine Engineering, University of Strathclyde, 100 Montrose Street, Glasgow, G4 0LZ, UK

ARTICLE INFO

Keywords:
Ship resistance
Roughness effect
Biofouling
Computational fluid dynamics (CFD)
Full-scale simulation
KRISO container ship (KCS)

ABSTRACT

To reduce the fuel consumption and green-house gas emissions of ships, it is necessary to understand the ship resistance. In this context, understanding the effect of surface roughness on the frictional resistance is of particular importance since the skin friction, which often takes a large portion in ship drag, increases with surface roughness. Although a large number of studies have been carried out since the age of William Froude, understanding the roughness effect is yet challenging due to its unique feature in scaling. In this study, a Computational Fluid Dynamics (CFD) based unsteady Reynolds Averaged Navier-Stokes (RANS) resistance simulation model was developed to predict the effect of barnacle fouling mainly on the resistance and hull wake characteristics of the full-scale KRISO container ship (KCS) hull. Initially, a roughness function model was employed in the wall-function of the CFD software to represent the surface conditions of barnacle fouling. A validation study was carried out involving the model-scale flat plate simulation, and then the same approach was applied in full-scale flat plate simulation and full-scale 3D KCS hull simulation for predicting the effect of barnacle fouling. The increase in frictional resistance due to the different fouling conditions were predicted and compared with the results obtained using the boundary layer similarity law analysis of Granville. Also, a further investigation of the roughness effect on the residuary resistance, viscous pressure resistance and wave making resistance was carried out. Finally, the roughness effect on the wave profile, pressure distribution along the hull, velocity distribution around the hull and wake flows were examined.

1. Introduction

To meet the needs of a globalized world, there has been a rapid expansion of maritime transportation. According to United Nations Conference on Trade and Development (UNCTAD, 2017), the seaborne trade volumes have more than tripled during the last four decades. While marine transport is considered more fuel-efficient than other freight methods, its greenhouse gas emissions are substantial and growing fast. The International Maritime Organization (IMO, 2014), forecasted maritime CO_2 emissions is to increase by 50%–250% in the period to 2050 depending on the scenarios of future economic and energy developments.

Within this framework, understanding further details of the ship resistance is important to minimize the fuel consumption and GHG emissions. Particularly, frictional resistance component plays an important role as it takes the largest portion of the total ship resistance for the majority merchant ships. For example, skin friction can account for up to 90% of the total resistance, for a slow-speed ship (Lackenby, 1962). The skin friction is critically affected by the surface roughness, as a proof, Schultz and Swain (2000) observed huge increases of 370% and 190% in skin friction due to the biofilm and algae in their experiment using a flow channel. Accordingly investigating the effect of hull fouling on ship resistance is of particular importance, to predict the increased ship resistance in-service.

A large number of experimental studies have been devoted to exploring the effect of surface roughness on skin friction over past 120 years, since the very first experimental investigation of the effect of hull roughness on a destroyer conducted by Froude (1872, 1874). As stated in Schultz and Swain (2000), there have been numerous studies to explore the adverse effect of marine coatings and biofouling on ship resistance by conducting various types of experimental methods including towing test of flat plates (McEntee, 1915; Benson et al., 1938; Lewkowicz and Das, 1986), rotating disk (Watanabe et al., 1969; Loeb et al., 1984; Candries et al., 2003), flow channel (Candries and Atlar, 2005; Andrewartha et al., 2010) or others (Kempf, 1937; Watanabe et al., 1969). The literature further indicates that the impact of calcareous fouling (e.g. barnacles) is particularly critical and greatly dependent on the type and coverage of fouling (McEntee, 1915; Kempf,

* Corresponding author.
E-mail address: soonseok.song@strath.ac.uk (S. Song).

https://doi.org/10.1016/j.oceaneng.2019.01.056
Received 24 October 2018; Received in revised form 29 January 2019; Accepted 30 January 2019

1937; Schultz, 2004, 2007).

More recently, there have been studies exploring the roughness effect of calcareous fouling. Demirel et al. (2017a) conducted a series of towing test using flat plates covered with 3D printed artificial barnacle patches and observed a 119% increase in skin friction due to the barnacles of varying sizes and coverages. Gowing et al. (2018) measured the drag of 3D printed panels of barnacles, oysters and tubeworms of varying spatial density and size scales, and the levels of fouling conditions were converted to the equivalent sand grain roughness. Womack et al. (2018) measured the boundary layer characteristics along idealized model barnacles in shape of truncated cones, and they found the equivalent sand grain roughness height and skin friction coefficients according to the densities of the model barnacles.

Although the detrimental impacts of the surface roughness on drag have been reported from the earliest times (Townsin, 2003), predicting the roughness effect on the full-scale ship is not an easy task owing to its unique feature in scaling. That is to say, the size of surface roughness cannot be downscaled proportionally to the model ship (Franzini, 1997).

The most widely used method to predict the roughness effect on full-scale ship resistance is the boundary layer similarity law scaling which was proposed by Granville (1958, 1978). The merit of using this method is that the full-scale roughness effect on an arbitrary length of the body covered with the same roughness can be predicted, once the roughness function, ΔU^+, of the surface is given. Since there is no universal roughness function for all types of roughness, the roughness functions of individual roughness types have to be obtained experimentally using the direct or indirect methods (Demirel, 2015). The indirect methods have been preferred by researchers to the direct methods since the indirect methods are generally simpler and more economical compare to the direct methods. Accordingly, there have been a large number of experimental studies to acquire roughness functions and the corresponding roughness Reynolds number, k^+, using the indirect methods derived by Granville (1958, 1978; 1982; 1987), including local method with displacement thickness (Schultz and Swain, 1999; Flack et al., 2005; Schultz et al., 2015), local method without displacement thickness (Karlsson, 1978), overall method (Schultz and Myers, 2003; Schultz, 2004; Shapiro, 2004; Demirel, 2015; Demirel et al., 2017a) or rotating disk method (Schultz and Myers, 2003; Holm et al., 2004). Schultz and Myers (2003) further concluded that the roughness functions obtained from the different indirect methods can bring a good agreement with the results obtained from the direct method.

These findings are valuable since the obtained roughness functions can be practically used for the prediction of the roughness effect at any length and speed of ship. Demirel (2015) utilized the roughness functions of marine coatings and biofouling to develop an in-house prediction code for the ship added resistance based on the boundary layer similarity law analysis of Granville (1958). Although Granville's similarity law scaling shows good agreement with full-scale ship trial results (Schultz, 2007), Granville's extrapolation method is still limited by the use of boundary layer analysis. That is to say, this method can only predict the roughness effect of given surface roughness on the frictional resistance of a flat plate of ship length and hence cannot consider the three-dimensional (3D) effect and inevitably it cannot examine the total resistance coefficients. Another restriction of this scaling method is that only one fixed roughness Reynolds number, k^+, and thus roughness function, ΔU^+, are taken into account in the calculation to represent the roughness effect on the whole flat plate, which is definitely not realistic as the local friction velocity, u_τ, varies by the flow being developed along the flat plate in reality (White, 2011).

Implementation of computational fluid dynamics (CFD) is an effective way to overcome the above-mentioned limits of boundary layer similarity law analysis. In CFD simulations the distribution of the local friction velocity, U_τ, is dynamically computed for each discretized cell, and therefore the dynamically varying roughness Reynolds number, k^+, and corresponding roughness function, ΔU^+, can be taken into account in the computation, and hence the roughness effect on ship resistance can be more accurately predicted (Demirel et al., 2017b). For this reason, there have been several studies investigating the roughness effect of marine coatings and biofouling on ship resistance using CFD simulations. Patel (1998) remarked that once the roughness function model, $\Delta U^+ = f(k^+)$, of the roughness type is known, the given roughness function model can be employed into the wall-function in the CFD so that the wall boundary condition in the simulation represents the roughness on the surface. Date and Turnock (1999) proposed a numerical approach modifying the wall-function coefficient to predict the roughness effect on frictional resistance of a flat plate, however their method cannot directly represent the viscous flow over rough surface as the dynamically changing values of ΔU^+, is not considered in the CFD computation. Izaquirre-Alza et al. (2010) conducted CFD simulation of a flat plate coated with marine coatings using SST k-ω turbulence model and showed a good agreement with the experimental result, however they did not provide any information about the roughness function model employed in their CFD model and valid evidence of the selection of the roughness height of the coatings. Eça and Hoekstra (2011) examined the effect of sand-grain roughness on skin friction of a ship-length flat plate and further asserted that the roughness can be accurately simulated using either wall-functions or near-wall resolution. However, there is a continuing concern by ITTC (2011a) in the use of sand grain roughness for prediction of ship resistance due to the dissimilar behaviour of closely packed sand grain roughness which is not found in real ship surface roughness. Demirel et al. (2014), on the other hand, developed a CFD model for the prediction of skin friction of antifouling coatings. They employed roughness functions obtained from a series of towing tests of flat plates coated with antifouling coatings (Schultz, 2004) and validated the modified wall-function approach by comparing the results obtained by CFD with the experimental data. They then applied the same approach to ship-length flat plate simulations to investigate the frictional resistance of the antifouling coatings.

There have been fewer studies carried out for the examination of the effect of the surface roughness on 3D hull shape. Castro et al. (2011) conducted full-scale simulations of the KRISO container ship (KCS) modifying the wall-function coefficients according to the roughness height of the coating. However, they used a fixed value of roughness function so that the simulation cannot accurately reflect the roughness effect due to the coating roughness as the case of Date and Turnock (1999). Recently, Demirel et al. (2017b), developed a CFD model to explore the roughness effect of marine coatings and biofouling on full-scale ship resistance. They conducted simulations of full-scale flat plate and KCS hull and compared the simulation results with the results obtained using similarity law analysis. Although they employed the roughness function model suggested by Schultz (2007) into the wall-function of the CFD software, they have not directly validated their results against any experimental data. As discussed above, it is still questionable if the surface boundary conditions of the existing CFD studies can realistically represent the surface roughness of real ships. Therefore, it is worth conducting a systematic analysis by employing a realistic surface boundary condition to predict the effect of hull fouling on ship performance.

To the best of the authors' knowledge, there exists no specific study to predict the effect of barnacles of varying sizes and coverages on the ship resistance components. Therefore, this study aims to fill this gap by developing a CFD model to simulate a realistic surface roughness through employing a roughness function model representing barnacle fouling and performing a comprehensive investigation on the roughness effect of barnacle fouling on ship hydrodynamic characteristics using the proposed CFD model. The main advantage of the proposed approach is that the CFD simulations enable extensive analysis on the hydrodynamic details of the turbulent flow over the rough surface of a ship in a fully non-linear way, which is not possible using boundary

layer similarity law analysis.

In this study, the roughness function of barnacle fouling obtained by Demirel et al. (2017a) was employed in the wall-function of the CFD model to simulate the surface roughness of barnacle fouling of varying sizes and coverages. Firstly, the use of the modified wall-function approach was validated against the experimental data. Then the same wall-function approach was used for full-scale flat plate simulations and 3D KCS hull simulations. The increase of frictional resistance due to the different fouling conditions were predicted and compared with the results obtained using boundary layer similarity law analysis. Finally, the roughness effect on the wave profile, pressure distribution along the hull, velocity distribution around the hull and its wake were examined.

1.1. Roughness effect on the turbulent boundary layer

The surface roughness causes an increase in the turbulence. As a consequence, the turbulent stress, wall shear stress and finally the skin friction increase. The roughness effect can also be observed in the velocity profile in the log-law region. Clauser (1954) showed that the roughness effect results in a downward shift in the velocity profile in the log-law region. This downward shift is termed as the 'Roughness Function', ΔU^+. The non-dimensional velocity profile in log-the law region for a rough surface is then given as

$$U^+ = \frac{1}{\kappa}\log y^+ + B - \Delta U^+ \tag{1}$$

The roughness function, ΔU^+ can be expressed as a function of the roughness Reynolds number, k^+, defined as

$$k^+ = \frac{kU_\tau}{\nu} \tag{2}$$

It should be borne in mind that ΔU^+simply vanishes in the case of a smooth condition. Once the roughness function, $\Delta U^+ = f(k^+)$, of a certain roughness surface is known, it can be utilized in the boundary layer similarity law analysis of Granville (1958, 1987) or directly embedded into a CFD solver to predict the roughness effect on the frictional resistance of a ship covered with the given roughness (Demirel et al., 2017b).

2. Methodology

2.1. Approach

Fig. 1 shows the flow chart of the methodology to achieve the aim of this study, i.e. the development of a CFD model to simulate the effect of barnacle fouling on a ship surface. Step 1 is employing the roughness function of the barnacle fouling into the wall-function in the CFD model so that the wall boundary condition can represent the rough surface due to barnacles. The roughness function and the corresponding roughness heights obtained by Demirel et al. (2017a) was selected and employed in the wall-function of the CFD model. Step 2 is the validation of the proposed wall-function. A model-scale flat plate covered with barnacles of varying sizes and coverages was simulated numerically. Then the simulation results were compared with the experimental result of Demirel et al. (2017a). Step 3 is involved by conducting full-scale CFD simulations using the modified wall-function approach to predict the effect of barnacle fouling on the ship resistance components. The frictional resistance coefficients were predicted for the KCS 3D hull and compared with the results obtained from the full-scale flat plate simulation of the same ship using CFD as well as the results for the same ship based on the Granville's similarity law scaling procedure. The roughness effect on the different resistance components were also examined using the results of KCS hull simulations. Finally, the roughness effect on the wave profile, pressure distribution along the hull, velocity distribution and boundary layer development around the hull, and on the wake flow were examined.

2.2. Roughness function of barnacle fouling

In this study, the roughness function of barnacle fouling obtained by Demirel et al. (2017a) was embedded into the wall-function of the CFD models so that the surface boundary condition of the hull can represent the barnacle fouled surface.

Demirel et al. (2017a) used an experimental approach to find the roughness function of barnacle fouling. The study was based on an extensive series of towing test of flat plates covered with artificial barnacle patches. Different sizes of real barnacles, categorised as small, medium and big regarding their size, were digitised using 3D scanning technology and 3D printed into artificial barnacle tiles. The barnacle tiles were then glued onto the surfaces of flat plates by differing the coverage area and the plates were towed at a range of speeds. From the analyses of the experimental results, they found that the roughness functions of the barnacle fouling can be expressed using the Colebrook type roughness functions of Grigson (1992), given by

$$\Delta U^+ = \frac{1}{\kappa}\ln(1 + k^+) \tag{3}$$

Table 1 compares the roughness length scales of barnacle fouling obtained by the experiment and Fig. 2 shows the roughness functions for the test surfaces. For further details about the experiment, one can

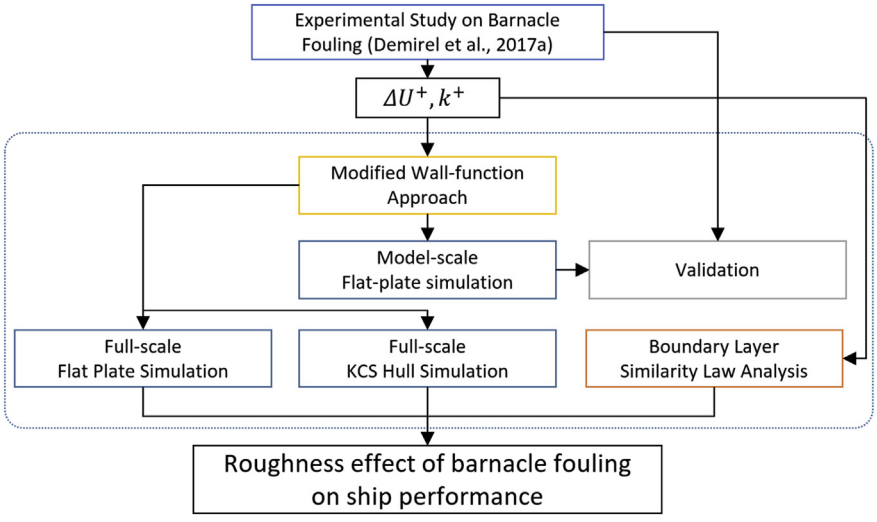

Fig. 1. The methodology followed in the study.

Table 1
Roughness length scales of test surfaces, adapted from Demirel et al. (2017a).

Test surface	Barnacle type	Surface coverage (%)	Barnacle height$h$ (mm)	Representative sand-grain roughness height k_G (μm)
B10%	Big	10%	5	174
B20%	Big	20%	5	489
M10%	Medium	10%	2.5	84
M20%	Medium	20%	2.5	165
M40%	Medium	40%	2.5	388
M50%	Medium	50%	2.5	460
S10%	Small	10%	1.25	24
S20%	Small	20%	1.25	63
S40%	Small	40%	1.25	149
S50%	Small	50%	1.25	194

refer the supplementary data in the online version, at https://doi.org/10.1080/08927014.2017.1373279.

2.3. Numerical modelling

2.3.1. Mathematical formulations

The proposed CFD model was developed based on the unsteady Reynolds-averaged Navier-Stokes (URANS) method using a commercial CFD software package, STAR-CCM+. The averaged continuity and momentum equations for incompressible flows may be given in tensor notation and Cartesian coordinates as in the following two equations (Ferziger and Peric, 2002).

$$\frac{\partial(\rho\bar{u}_i)}{\partial x_i} = 0 \tag{4}$$

$$\frac{\partial(\rho\bar{u}_i)}{\partial t} + \frac{\partial}{\partial x_j}(\rho\bar{u}_i\bar{u}_j + \rho\overline{u_i' u_j'}) = -\frac{\partial\bar{p}}{\partial x_i} + \frac{\partial\bar{\tau}_{ij}}{\partial x_j} \tag{5}$$

in which, ρ is density, $\bar{u}_i$ is the averaged velocity vector, $\rho\overline{u_i' u_j'}$ is the Reynolds stress, $\bar{p}$ is the averaged pressure, $\bar{\tau}_{ij}$ is the mean viscous stress tensor components. This viscous stress for a Newtonian fluid can be expressed as

$$\bar{\tau}_{ij} = \mu\left(\frac{\partial\bar{u}_i}{\partial x_j} + \frac{\partial\bar{u}_j}{\partial x_i}\right) \tag{6}$$

where μ is the dynamic viscosity.

In the CFD solver, the computational domains were discretized and solved using a finite volume method. The second-order upwind convection scheme and a first-order temporal discretization were used for the momentum equations. The overall solution procedure was based on a Semi-Implicit Method for Pressure-Linked Equations (SIMPLE) type algorithm.

The shear stress transport (SST) k-ω turbulence model was used to predict the effects of turbulence, which combines the advantages of the k-ω and the k-ε turbulence model. This model uses a k-ω formulation in the inner parts of the boundary layer and a k-ε behaviour in the free-stream for a more accurate near wall treatment with less sensitivity of inlet turbulence properties, which brings a better prediction in adverse pressure gradients and separating flow (Menter, 1994). A second-order convection scheme was used for the equations of the turbulent model.

For the models where free surfaces are present (model-scale flat plate and full-scale KCS hull simulations), the Volume of Fluid (VOF) method was used with High Resolution Interface Capturing (HRIC).

2.3.2. Geometry and boundary conditions

In the study, three different CFD models were generated, using the modified wall-function approach, to study the effect of the barnacle fouling, and these included: (i) Model-scale flat plate simulations for the validation; (ii) Full-scale flat plate representation of the KCS hull; (iii) Full-scale 3D simulations of the KCS hull appended with a rudder.

For all CFD models, the surface boundary conditions of the plates and ship hulls were defined as the no-slip condition. For smooth cases, the smooth type wall-function was used, while the fouled cases used the rough type wall-function containing the roughness function model, corresponding equations (1) and (3), for the boundary condition of the hull.

Fig. 3 shows the dimensions and boundary conditions used for the

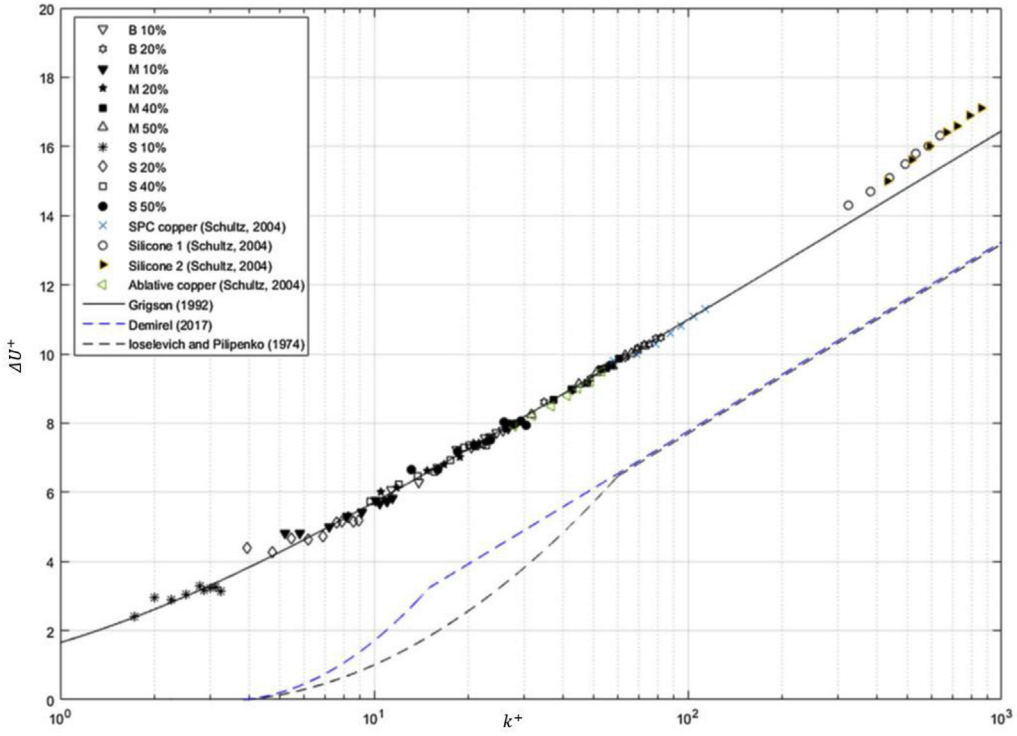

Fig. 2. Roughness functions for the test surfaces, adapted from Demirel et al. (2017a).

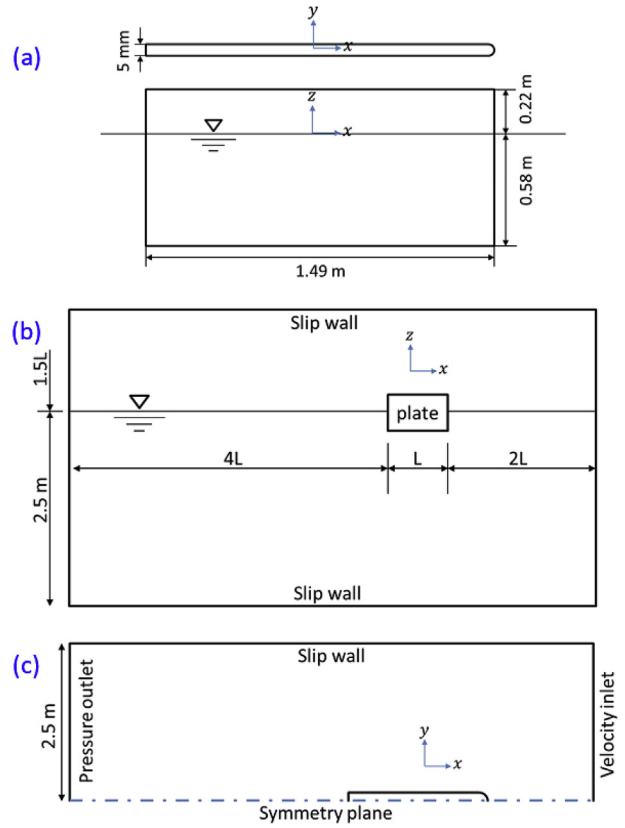

Fig. 3. The dimensions and boundary conditions for the model-scale flat plate simulation model, (a) the plate, (b) profile view of the computational domain, (c) top view of the computational domain.

model-scale flat plate simulation. The dimensions of the plate and the domain were selected to represent the towing test of Demirel et al. (2017a). For the boundary condition of the side wall and bottom of the towing tank, the slip-wall boundary condition was chosen to specify the flow field in the coordinate system fixed on the plate. For the two opposite faces at the x-direction, a velocity inlet boundary condition was applied for the inlet free-stream boundary condition, and a pressure outlet was chosen for the outlet boundary condition. In order to save the computational time, a symmetry boundary condition was applied on the vertical centre plane ($y = 0$), so that only a half of the plate and the control volume were taken into account. The authors believe that this does not significantly affect the results.

Fig. 4 shows the dimensions and boundary conditions used for the full-scale flat plate simulation. The length of the full-scale flat plate was chosen to represent the length of the KCS so that the roughness effect at the same Reynolds number of the KCS at its design speed (24 knots) and slow streaming speed (19 knots) can be examined. The full-scale plate simulation was modelled as fully submerged by defining the boundary conditions of horizontal and vertical centre planes ($z = 0$ and $y = 0$, respectively) as the symmetry planes. As a consequence, only a quarter of the plate and fluid domain was taken into account in order to save the computational time.

Table 2 shows the principal particulars of the KCS used in the full-scale KCS hull simulation. The body plan, and side profiles of KCS, the boundary conditions and the dimensions of the computational domain are shown in Fig. 5. The velocity inlet and pressure outlet boundary conditions were applied as the inlet and outlet boundary conditions. For the representation of deep water and infinite air conditions, the boundary conditions of the side walls, bottom and top of the domain were set to the velocity inlet, as similarly used by Demirel et al. (2017b). The vertical centre plane was defined as the symmetry plane,

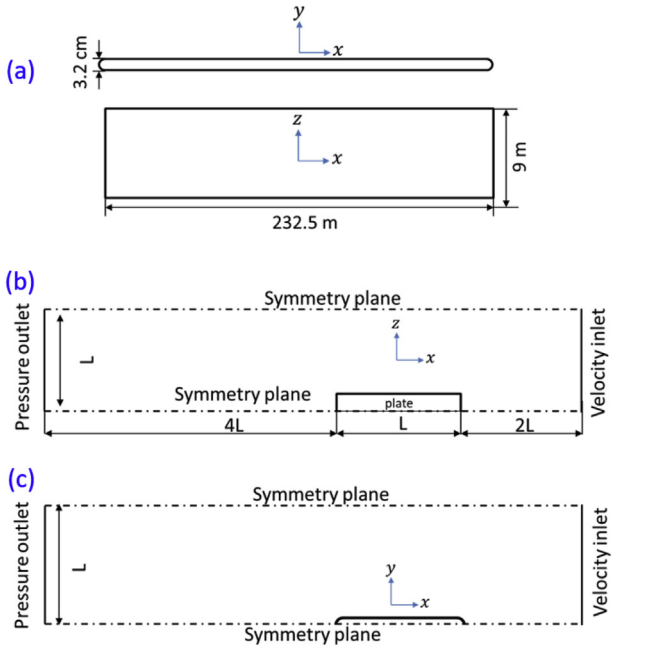

Fig. 4. The dimensions and boundary conditions for the full-scale flat plate simulation model, (a) the plate, (b) profile view of the computational domain, (c) top view of the computational domain.

Table 2
Principal particulars of the KCS in full-scale and model-scale, adapted from Kim et al. (2001) and Larsson et al. (2013)

Length between the perpendiculars	L_{BP} (m)	230
Length of waterline	L_{WL} (m)	232.5
Beam at waterline	B_{WL} (m)	32.2
Depth	D (m)	19.0
Design draft	T (m)	10.8
Wetted surface area with a rudder	S (m^2)	9539
Displacement	∇ (m^3)	52030
Block coefficient	C_B	0.6505
Design speed	V (knot, m/s)	24
Froude number	F_n	0.26
Propeller diameter	D_p (m)	7.9
Hub ratio	D_h/D_p	0.18

and hence only a half of the domain was taken into account. It is important to note that the full-scale KCS simulations were conducted in a fixed condition, such that the ship was not allowed to sink or trim in the simulations.

2.3.3. Mesh generation

Mesh generation was performed using the built-in automated mesh tool of STAR-CCM+. Trimmed hexahedral meshes were used for the high-quality grid for the complex domains. Local refinements were made for finer grids in the critical regions, such as the areas around the body, near the free surface, leading and trailing edges, the rudder and bulbous bow of the hull.

The prism layer meshes were used for near-wall refinement, and the thickness of the first layer cell on the surface was chosen such that the y^+ value is always higher than 30, and higher than k^+ value, as suggested by Demirel et al. (2017b), Owen et al. (2018), and CD-Adapco (2017). Fig. 6 shows the volume meshes on the cross-sections of the domain.

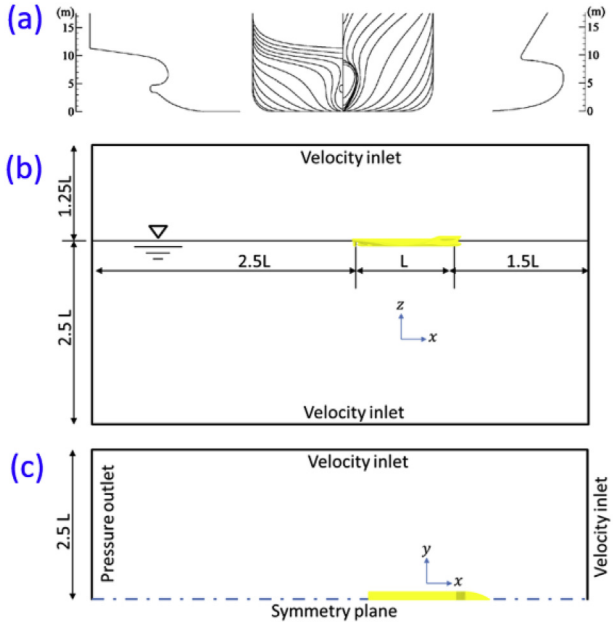

Fig. 5. The dimensions and boundary conditions for the full-scale KCS hull simulation model, (a) body plane and side profiles of the KCS, adapted from Kim et al. (2001), (b) profile view of the computational domain, (c) top view of the computational domain.

3. Results

3.1. Verification study

A verification study was conducted to assess the numerical uncertainties of the CFD models and to determine sufficient grid-spacing and time step. The Grid Convergence Index (GCI) method based on the extrapolation of Richardson (1910) was used to estimate the order of accuracy of the simulations. It is of note that, although the GCI method was firstly intended to be used for spatial convergence studies, it can also be used for a temporal convergence study as shown in Tezdogan et al. (2015) and Terziev et al. (2018).

According to Celik et al. (2008) the apparent order of the method, p_a, is determined by

$$p_a = \frac{1}{\ln(r_{21})} |\ln \left| \frac{\varepsilon_{32}}{\varepsilon_{21}} \right| + q(p_a)| \tag{7}$$

$$q(p_a) = \ln\left(\frac{r_{21}^{p_a} - s}{r_{32}^{p_a} - s} \right) \tag{8}$$

$$s = sign\left(\frac{\varepsilon_{32}}{\varepsilon_{21}} \right) \tag{9}$$

where, r_{21} and r_{32} are refinement factors given by $r_{21} = \sqrt[3]{N_1/N_2}$ for a spatial convergence study of a 3D model, or $r_{21} = \Delta t_1/\Delta t_2$ for a temporal convergence study. N and Δt are the cell number and time step, respectively. $\varepsilon_{32} = \phi_3 - \phi_2$, $\varepsilon_{21} = \phi_2 - \phi_1$, and ϕ_k denotes the key variables, i.e. C_T in this study.

The extrapolated value is calculated by

$$\phi_{ext}^{21} = \frac{r_{21}^p \phi_1 - \phi_2}{r_{21}^p - 1} \tag{10}$$

The approximate relative error, e_a^{21}, and extrapolated relative error, e_{ext}^{21}, are then obtained by

$$e_a^{21} = \left| \frac{\phi_1 - \phi_2}{\phi_1} \right| \tag{11}$$

$$e_{ext}^{21} = \left| \frac{\phi_{ext}^{21} - \phi_1}{\phi_{ext}^{21}} \right| \tag{12}$$

Finally, the fine-grid convergence index is found by

$$GCI_{fine}^{21} = \frac{1.25 e_a^{21}}{r_{21}^p - 1} \tag{13}$$

3.1.1. Spatial convergence study

For spatial convergence study, three different resolutions of meshes were generated, which are referred to as fine, medium, and coarse meshes corresponding the cell numbers of N_1, N_2, and N_3. Table 3 shows the required parameters for the calculation of the spatial discretization error. The total resistance coefficient values, C_T, of smooth cases were used as the key variables. The inlet velocity for the model-scale flat plate simulation was set to $V = 2.435\ m/s$ which is one of the towing speeds of Demirel et al. (2017a), while the inlet velocity of 24 knots was used for the simulations of full-scale flat plate and KCS hull. As indicated in the table, the numerical uncertainty of fine meshes (GCI_{fine}^{21}) for the model-scale flat plate, full-scale flat plate and KCS hull CFD models are 0.77%, 0.11% and 0.96% respectively. For accurate prediction of the roughness effect of barnacle fouling, the fine mesh of each case was used in this study.

3.1.2. Temporal convergence study

For the temporal convergence study, three different time steps, namely Δt_1, Δt_2, and Δt_3, were applied to the simulations using fine meshes. Table 4 shows the required parameters for the calculation of the temporal discretization error. The total resistance coefficient values, C_T, of smooth cases were used as the key variable. The inlet velocity for the model-scale flat plate simulation was set to $V = 2.435\ m/s$ which is one of the towing speeds of Demirel et al. (2017a), while the inlet velocity of 24 knots was used for full-scale flat plate and the KCS hull simulations. As indicated in the table, the numerical uncertainties of the smallest time steps ($GCI_{\Delta t_1}^{21}$) of the model-scale flat plate, full-scale flat plate, and KCS hull CFD models are 0.01%, 0.002% and 0.65% respectively. For accurate prediction of the roughness effect of barnacle fouling on ship resistance, the smallest time step, Δt_1, of each model was used in this study. It is of note that the recommended time step by ITTC (2011b) is $0.005 \sim 0.01 L/V$, and the time steps used in this study were within this range or even smaller.

3.2. Validation study

3.2.1. Validation of the CFD models in smooth condition

To validate the CFD models in smooth condition, the C_T values obtained using the CFD simulations were compared with the experimental data of Demirel et al. (2017a) and the extrapolated result using the experimental data of Kim et al. (2001). The inlet velocity of model-scale flat plate simulation was set to $V = 2.435\ m/s$ ($Rn = 2.8 \times 10^6$), which is one of the towing speeds of Demirel et al. (2017a), while the design speed of the KCS was used for the full-scale KCS hull simulation. The density and dynamic viscosity of fresh water at 15 °C and sea water at 20 °C were used for the model-scale flat plate simulation and the full-scale KCS simulation, respectively. The full-scale C_T value used for the comparison were extrapolated using the frictional resistance coefficient, C_F, obtained from ITTC 1957 friction line (ITTC, 2011c) and the residuary resistance, C_R, obtained by Kim et al. (2001). As can be seen in Table 5, the model-scale flat plate and full-scale KCS hull simulation results show good agreement with the experimental results, showing relative errors of 0.38% and 0.54% respectively.

Figs. 12 and 13 show the wave profiles obtained from the simulations and the experiment of Kim et al. (2001). To examine the scale effect together, the wave profiles obtained from model-scale simulations ($L_{PP} = 7.286m$) are also included in the figures. As can be seen from Fig. 12, a good agreement was achieved between the wave profiles

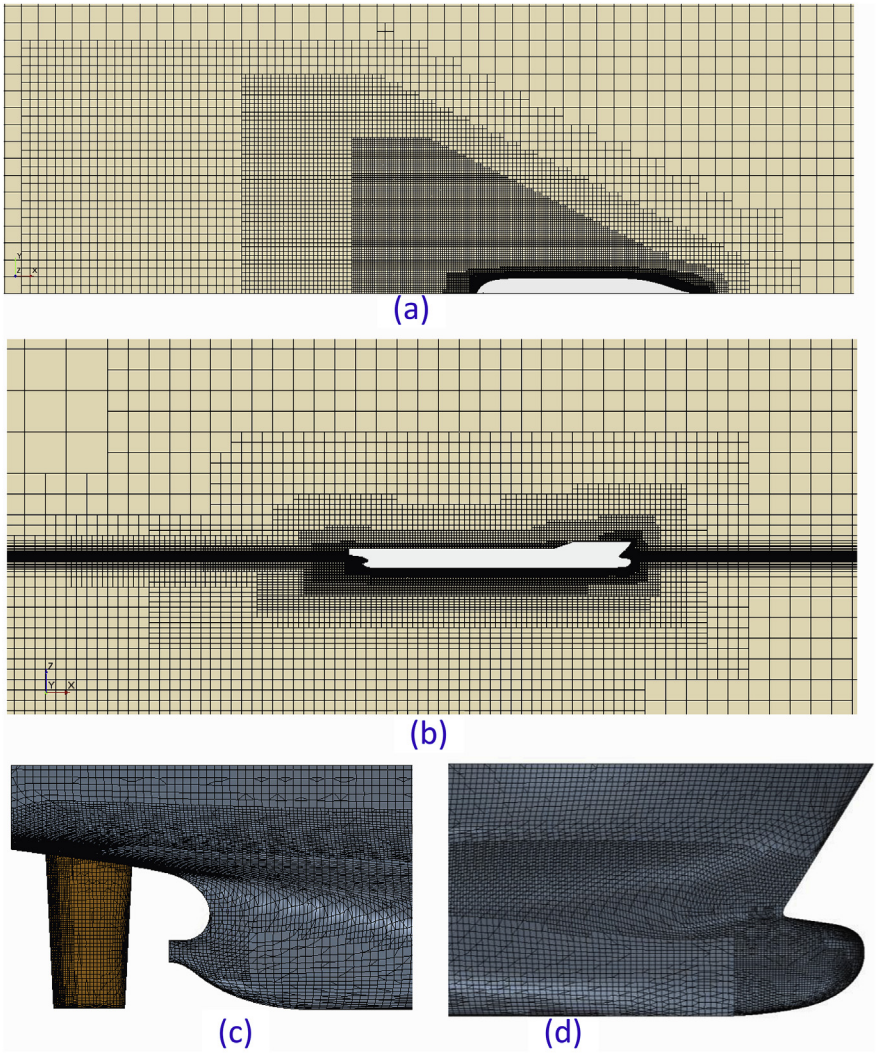

Fig. 6. Volume mesh of full-scale KCS hull simulation model, (a) top view, (b) profile view, (c) stern refinement, (d) bow refinement.

Table 3
Parameters used for the calculation of the discretization error for the spatial convergence study, key variable: C_T.

	Model-scale flat plate	Full-scale flat plate	Full-scale KCS hull
N_1	2,300,000	1,200,000	2,000,000
N_2	930,000	850,000	1,300,000
N_3	460,000	610,000	630,000
r_{21}	1.35	1.12	1.26
r_{32}	1.26	1.12	1.42
ϕ_1	3.981E-03	1.357E-03	2.095E-03
ϕ_2	4.021E-03	1.355E-03	2.103E-03
ϕ_3	4.092E-03	1.347E-03	2.126E-03
ε_{32}	7.16E-05	−7.94E-06	2.27E-05
ε_{21}	3.98E-05	−2.62E-06	8.67E-06
s	1	1	1
e_a^{21}	1.00%	0.19%	0.41%
q	3.74E-01	6.50E-02	−5.34E-01
p_a	3.19E+00	1.02E+01	1.86E+00
ϕ_{ext}^{21}	3.956E-03	1.358E-03	2.078E-03
e_{ext}^{21}	0.62%	−0.09%	0.78%
GCI_{fine}^{21}	0.77%	0.11%	0.96%

Table 4
Parameters of the calculation of the discretization error for the temporal convergence study, key variable: C_T

	Model-scale flat plate	Full-scale flat plate	Full-scale KCS hull
Δt_1	0.01s	0.16s	0.02s
Δt_2	0.02s	0.32s	0.04s
Δt_3	0.04s	0.64s	0.08s
r_{21}, r_{32}	2	2	2
ϕ_1	3.981E-03	1.357E-03	2.095E-03
ϕ_2	3.980E-03	1.357E-03	2.108E-03
ϕ_3	3.978E-03	1.360E-03	2.136E-03
ε_{32}	−2.58E-06	2.77E-06	2.88E-05
ε_{21}	−8.80E-07	2.50E-07	1.31E-05
e_a^{21}	0.02%	0.018%	0.62%
p_a	1.55E+00	3.47E+00	1.14E+00
ϕ_{ext}^{21}	3.982E-03	1.357E-03	2.084E-03
e_{ext}^{21}	−0.01%	0.0018%	0.52%
$GCI_{\Delta t_1}^{21}$	0.01%	0.0023%	0.65%

along the hull obtained from the current CFD models and the EFD data. On the other hand, as shown in Fig. 13a, differences were observed from the full-scale wave profile along a line with constant $y = 0.1509L_{pp}$. The wave profile of the full-scale simulation in smooth condition shows larger elevation at downstream region of the ship compare to those of the model-scale simulation and EFD data. Considering that the model-scale CFD simulation shows good agreement with the EFD data (Fig. 13b), this difference can be most attributed to the different Reynolds numbers of the full-scale CFD and the model-

Table 5
values obtained from the CFD simulations and the experiments.

	C_T		
	Simulation	Experiment	Relative error
Model-scale flat plate	3.981E-03	3.397E-03[a]	0.38%
Full-scale KCS hull	2.095E-03	2.083E-03[b]	0.54%

[a] Experimental data of Demirel et al. (2017a).
[b] Extrapolated using the experimental data of Kim et al. (2001).

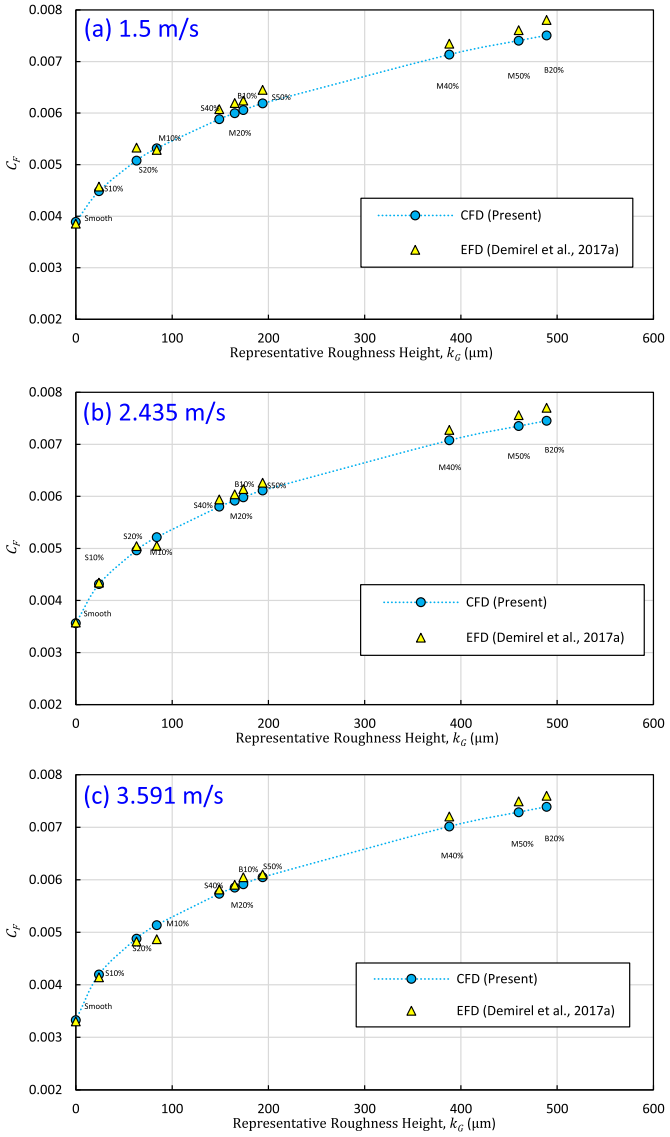

Fig. 7. C_F values of flat plates towed with different fouling conditions obtained from the simulations and the experiments by Demirel et al. (2017a), (a) $V_{inlet} = 1.5m/s$, (b) $V_{inlet} = 2.435m/s$, (c) $V_{inlet} = 3.591m/s$

scale EFD, as similarly observed by Castro et al. (2011) and Demirel et al. (2017b).

3.2.2. Validation of the modified wall-function approach

Fig. 7 compares the C_F values of model-scale flat plates in different fouling conditions computed from the CFD simulations with the experimental data of Demirel et al. (2017a). The horizontal axes of the figures indicate the corresponding roughness heights, k_G, of the barnacle fouling conditions given in Table 1. It is evident from the figure that a good agreement is achieved between the current CFD model and the experiment of Demirel et al. (2017a). This suggests that the modified wall-function approach implemented in the CFD model can accurately represent the surface roughness of barnacle fouling. Therefore, it can be used to investigate the effect of barnacle fouling on the hydrodynamic characteristics of ships.

3.3. Roughness effect on full-scale ship resistance components

Before investigating the roughness effect on the ship resistance components, it would be appropriate to re-state the major components. The total resistance, R_T, of a ship can be divided into two main components; the frictional resistance, R_F, and the residuary resistance, R_R, given by

$$R_T = R_F + R_R \tag{14}$$

The frictional resistance arises from the friction between the fluid and the hull surface while the residuary resistance is pressure related resistance consisting of viscous pressure resistance R_{VP}, and wave making resistance R_W, given by

$$R_T = R_F + R_{VP} + R_W \tag{15}$$

The viscous pressure or also known as form drag is broadly assumed to be proportional to the frictional resistance (Lewis, 1988), with the use of form factor, k, as given

$$R_{VP} = kR_F \tag{16}$$

$$R_T = (1 + k)R_F + R_W \tag{17}$$

The resistance components can be non-dimensionalized by dividing each term by the dynamic pressure, $\frac{1}{2}\rho V^2$, and the wetted surface area of the ship hull, S. The resistance coefficients can be defined as

$$C_T = C_F + C_R \tag{18}$$

$$C_T = C_F + C_{VP} + C_W \tag{19}$$

$$C_T = (1 + k)C_F + C_W \tag{20}$$

where, C_T, C_F, and C_R are the coefficients of total, frictional and residuary resistance, respectively.

For the investigation into the effect of barnacle fouling on full-scale ship resistance and powering, full-scale flat plate CFD simulation and KCS hull simulation were conducted using the modified wall-function approach proposed in this study. The simulations were conducted at the design speed of 24 knots and slow steaming speed of 19 knots, whose corresponding Reynolds numbers are 2.7×10^9 and 2.1×10^9, respectively.

3.3.1. Total resistance and effective power

The total resistance coefficients, C_T, were obtained from the full-scale KCS hull simulations in the surface conditions of varying sizes and coverage of barnacle fouling. As indicated in Table 6 the C_T values show

Table 6
values obtained from full-scale KCS hull simulation.

Test Surface	k_G (μm)	24 knots		19 knots	
		C_T	ΔC_T, ΔP_E	C_T	ΔC_T, ΔP_E
Smooth	0	2.095E-03	0%	1.803E-03	0%
S10%	24	2.475E-03	18%	2.192E-03	22%
S20%	63	2.691E-03	28%	2.419E-03	34%
M10%	84	2.767E-03	32%	2.498E-03	39%
S40%	149	2.936E-03	40%	2.670E-03	48%
M20%	165	2.968E-03	42%	2.704E-03	50%
B10%	174	2.985E-03	42%	2.724E-03	51%
S50%	194	3.020E-03	44%	2.760E-03	53%
M40%	388	3.265E-03	56%	3.018E-03	67%
M50%	460	3.333E-03	59%	3.088E-03	71%
B20%	489	3.358E-03	60%	3.114E-03	73%

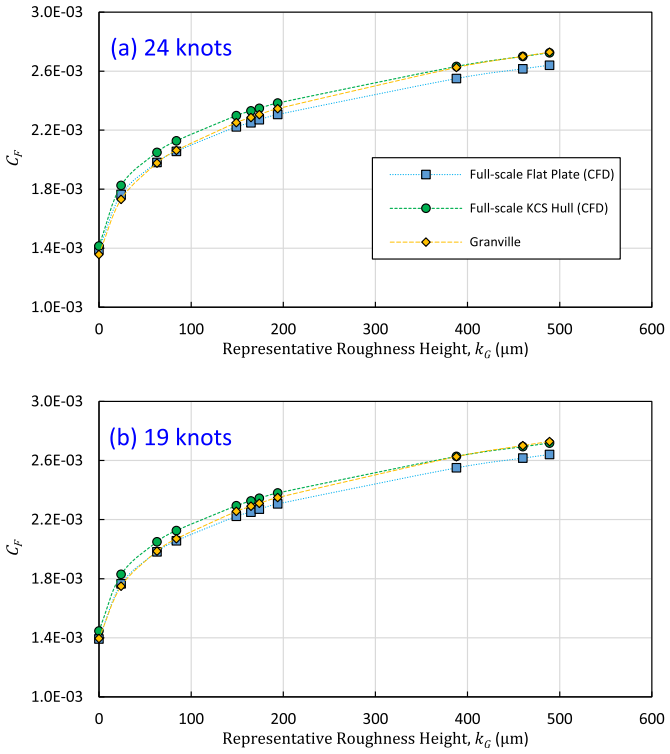

Fig. 8. values obtained by the proposed full-scale CFD simulations and Granville's similarity law extrapolation at (a) 24knots and (b) 19knots.

a significant increase due to the barnacle fouling. The increase in total resistance and the effective power of the ship was observed to be higher at 19 knots than 24 knots (by 73% and 60%, respectively). It can be attributed to the fact that the contribution of the frictional resistance becomes more dominant in the total resistance at lower speeds, and it is believed that the surface roughness mainly affects the frictional resistance rather than other resistance components. For these reasons, it appears that the effect of surface roughness on ship total resistance is more dominant at lower speeds. Therefore, it is worth investigating the effect of barnacle fouling on different resistance components.

3.3.2. Frictional resistance and residuary resistance

The frictional resistance coefficients and residuary resistance coefficients were directly computed from the full-scale KCS hull simulations and flat plate simulation. Additionally, the simulation results were compared with the C_F values of flat plates with the same length as the KCS, extrapolated using Granville's boundary layer similarity law scaling method (Granville, 1958, 1987).

Fig. 8 shows the frictional resistance coefficients, C_F, obtained from the two full-scale simulations and similarity law analysis at the design speed of 24 knots and slow steaming speed of 19 knots. In the figure, the C_F values are plotted against the representative roughness heights, k_G, of the corresponding fouling conditions. As can be seen in the figure, the frictional resistance coefficients obtained using the three different methods show excellent agreements in trends and with close values in magnitudes at both speeds. It appears that due to the three-dimensional effect, the C_F values of the 3D KCS hull simulations are always higher than those of flat plate simulations.

Table 7 compares the frictional resistance coefficients, the percentage of added resistance and the residuary resistance coefficients, C_R, obtained from the 3D full-scale KCS hull simulations with different fouling conditions at 24 knots and 19 knots. The increase in the C_F values of KCS due to the fouling conditions was predicted to be up to 93% and 88% in the most severe fouled conditions (B20% case) at the design speed and slow streaming speed, respectively. It is notable that only with 10% coverage of small barnacle (S10% case) fouling can result in nearly 30% increase in the frictional resistance of KCS at the design speed.

It is also not surprising that the C_F values of the fouled cases (except S10%) remain rather consistent with the increasing speed (from 19 knots to 24 knots), while the smooth C_F is decreasing. This is due to the fact that the C_F starts to lose its dependency to the Reynolds number when it approaches to the fully rough regime (Moody, 1944). For the same reason, the percentage of the increased C_F appear higher at 24 knots than 19 knots, as only C_F in the smooth case decreases with the increase of Reynolds number while C_F of rough surfaces remain relatively consistent.

On the other hand, interesting features were observed in residuary resistance, C_R, between the two speeds. As can be seen in Fig. 9, the C_R values of the KCS at 24 knots showed decreasing trend with increasing fouling rate, while it tended to decrease as the roughness height increases at 19 knots. It appears that this difference arises from the different portions of viscous pressure resistance, C_{VP}, and wave making resistance, C_W, at different speeds as firstly found in Demirel et al. (2017b). Further discussion of the roughness effect on C_{VP} and C_W can be found in section 3.3.3.

3.3.3. Viscous pressure and wave making resistance

To investigate the rationale behind the different trend of the residuary resistance at different speeds, the residuary resistance coefficients were divided into the viscous pressure resistance coefficients, C_{VP}, and wave making resistance coefficients, C_W. To find the equivalent form factors, k, double-body flow calculation was conducted by modifying the CFD models. In the double-body simulations, the free surface is replaced by a symmetry plane so that no wave can be generated and hence only the frictional resistance and the viscous pressure resistance exist (Raven et al., 2008). Table 8 shows the form factors, k, of the KCS obtained from the double-body simulations at the design speed (24 knots) and slow steaming speed (19 knots). As can be seen from the table, the k values were observed to decrease as the surface roughness increases, and therefore the increase of C_{VP} due to the surface roughness is not proportional to C_F, which disagrees with the assumptions of Lewis (1988) and Demirel et al. (2017b).

Fig. 10 illustrates the values of C_R, C_{VP} and C_W varying with the fouling rate. It is apparent that the wave making resistance, C_W, of the KCS decreases as the level of hull fouling increases, whilst the viscous pressure resistance, C_{VP}, increases with the increasing fouling rate. Since C_R is sum of C_{VP} and C_W, C_R can increase or decrease depending on the dominance of C_{VP} and C_W. Therefore, the full-scale C_R values at 24 knots show decreasing trend with increasing surface fouling an due to the dominance of C_W while they show increasing trend at 19 knots due to the relatively small portion of C_W.

3.3.4. Contribution of resistance components

Since it was found in the previous sections that the effect of surface roughness varies in each resistance component, it is worth investigating the change in the portions of resistance components due to barnacle fouling. Fig. 11 compares the percentages of the resistance components in different surface conditions at the two speeds. The portions of C_F values increase from 68% to 81% at 24 knots and from 80% to 87% at and 19 knots. On the other hand, the percentage of C_{VP} in total resistance tends to remain rather stable for both speeds, while the percentage of C_W rapidly decrease from 24% to 11% at 24 knots, and from 10% to 4% at 19 knots. As discussed in section 3.3.1 the frictional resistance coefficients are more dominant at 19 knots, and result in larger increases in total resistance as the surface roughness increases.

3.4. Wave profile

As it was found that the surface roughness of the KCS affects the wave making resistance, it is worth examining the roughness effect on

Table 7
Comparison of the frictional resistance coefficients and the residuary resistance coefficients computed from the full-scale KCS hull simulations at 24 knots and 19 knots.

Surface condition	k_G (μm)	24 knots				19 knots			
		C_F	ΔC_F	C_R	ΔC_R	C_F	ΔC_F	C_R	ΔC_R
Smooth	0	1.415E-03	0%	6.792E-04	0.0%	1.446E-03	0%	3.565E-04	0.0%
S10%	24	1.826E-03	29%	6.489E-04	−4.5%	1.829E-03	26%	3.632E-04	1.9%
S20%	63	2.050E-03	45%	6.409E-04	−5.6%	2.049E-03	42%	3.697E-04	3.7%
M10%	84	2.128E-03	50%	6.395E-04	−5.8%	2.126E-03	47%	3.716E-04	4.2%
S40%	149	2.299E-03	62%	6.371E-04	−6.2%	2.294E-03	59%	3.766E-04	5.6%
M20%	165	2.331E-03	65%	6.365E-04	−6.3%	2.326E-03	61%	3.779E-04	6.0%
B10%	174	2.348E-03	66%	6.363E-04	−6.3%	2.345E-03	62%	3.791E-04	6.3%
S50%	194	2.384E-03	68%	6.357E-04	−6.4%	2.380E-03	65%	3.799E-04	6.6%
M40%	388	2.632E-03	86%	6.334E-04	−6.7%	2.628E-03	82%	3.906E-04	9.6%
M50%	460	2.700E-03	91%	6.331E-04	−6.8%	2.693E-03	86%	3.943E-04	10.6%
B20%	489	2.725E-03	93%	6.335E-04	−6.7%	2.718E-03	88%	3.956E-04	11.0%

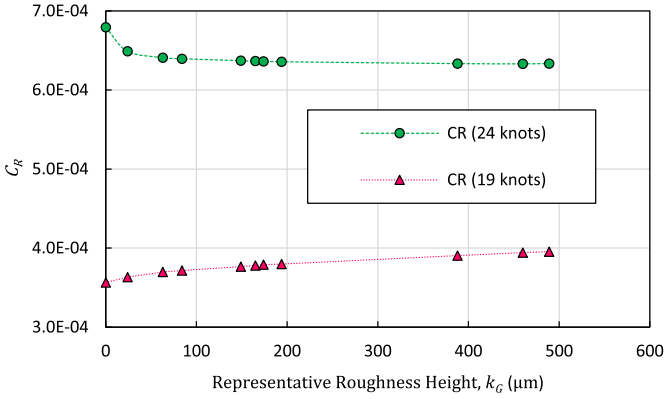

Fig. 9. Residuary resistance coefficients versus roughness heights, obtained from full-scale KCS hull simulations at 24 knots and 19 knots.

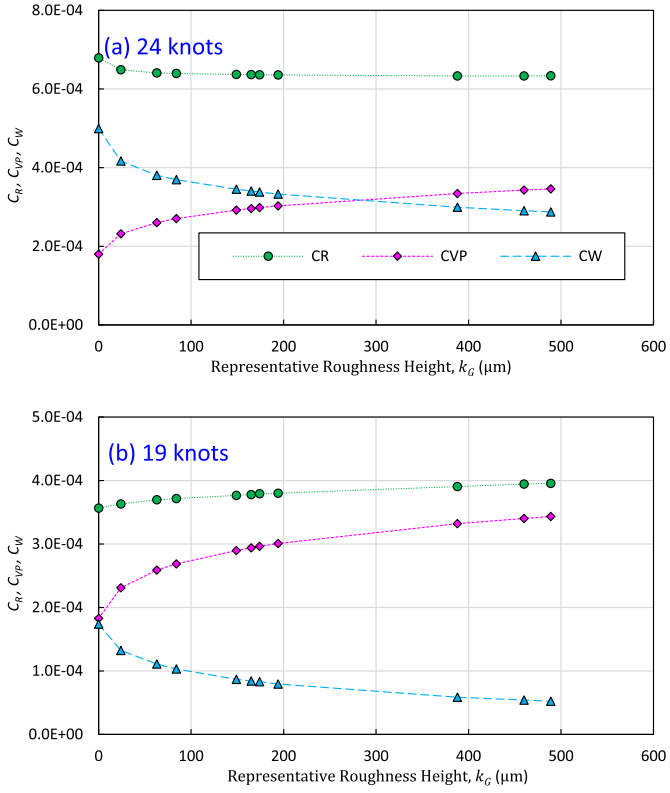

Fig. 10. Comparison of the residuary resistance, viscous pressure resistance and wave making resistance versus the representative roughness height of the fouling conditions, (a) 24 knots, (b) 19 knots.

wave profiles of the KCS. Fig. 12 compares the wave profile along the hull of the KCS in the smooth case and the rough case (B20%), and it also includes the wave profiles obtained from model-scale simulations ($L_{PP} = 7.286m$). As illustrated in the figure similar wave profiles were recorded for different surface conditions in both scales. In contrast, differences were observed in the wave profile along a line with $y = 0.1509L_{pp}$, as shown in Fig. 13. In both scales, the wave profiles of the smooth and rough cases collapse on top of each other for $x > -0.25L_{pp}$ and then deviate from each other in the region downstream of the ship. This observation suggests that the roughness effect on the ship wave is minor with the exception of the wake region where the viscous effects become important (Castro et al., 2011). The reduced wave elevation observed at the wake region by the roughness effect is in accordance with the finding of decreasing trend of C_W with increasing

Table 8
Form factor calculation from the double-body simulations.

Surface condition	k_G (μm)	24 knots				19 knots			
		C_T	C_F	k	Δk	C_T	C_F	k	Δk
Smooth	0	1.511E-03	1.341E-03	0.1268	0%	1.547E-03	1.374E-03	0.1259	0%
S10%	24	1.959E-03	1.759E-03	0.1137	−10%	1.965E-03	1.765E-03	0.1133	−10%
S20%	63	2.194E-03	1.978E-03	0.1092	−14%	2.198E-03	1.981E-03	0.1095	−13%
M10%	84	2.275E-03	2.054E-03	0.1076	−15%	2.278E-03	2.056E-03	0.1080	−14%
S40%	149	2.452E-03	2.218E-03	0.1055	−17%	2.454E-03	2.220E-03	0.1054	−16%
M20%	165	2.486E-03	2.250E-03	0.1049	−17%	2.488E-03	2.251E-03	0.1053	−16%
B10%	174	2.504E-03	2.266E-03	0.1050	−17%	2.506E-03	2.268E-03	0.1049	−17%
S50%	194	2.541E-03	2.301E-03	0.1043	−18%	2.543E-03	2.302E-03	0.1047	−17%
M40%	388	2.800E-03	2.541E-03	0.1019	−20%	2.802E-03	2.542E-03	0.1023	−19%
M50%	460	2.869E-03	2.605E-03	0.1013	−20%	2.871E-03	2.606E-03	0.1017	−19%
B20%	489	2.895E-03	2.629E-03	0.1012	−20%	2.897E-03	2.630E-03	0.1015	−19%

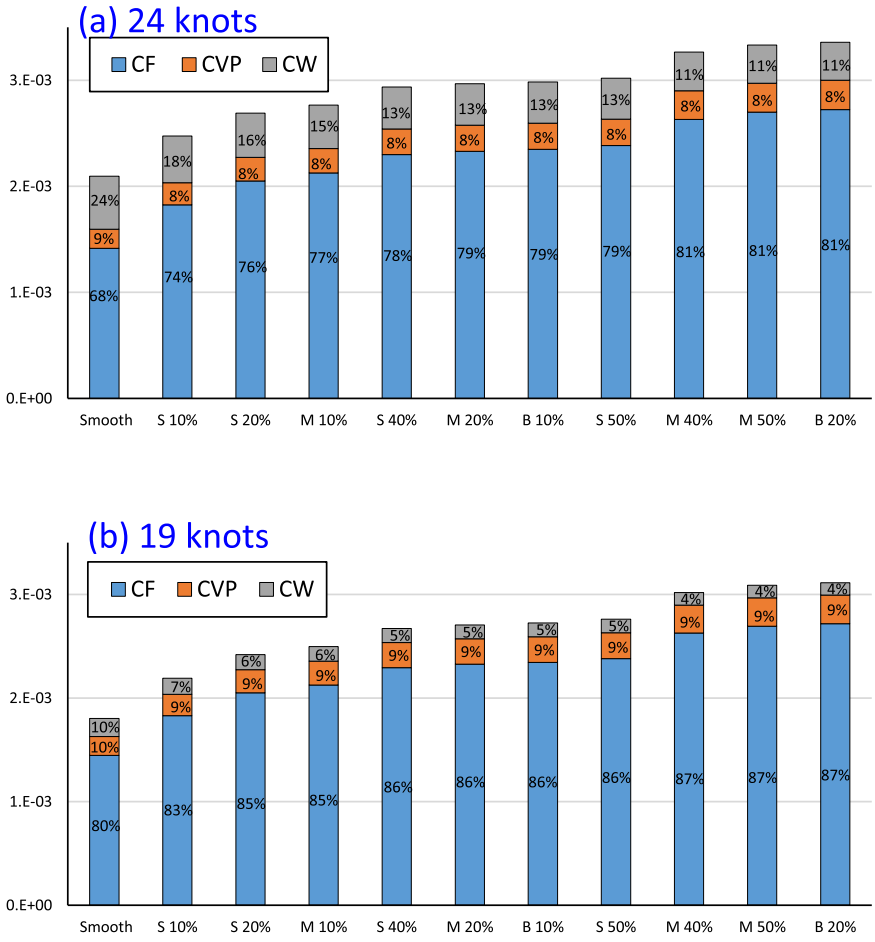

Fig. 11. Percentage bar diagram of the resistance components, at (a) 24 knots, (b) 19 knots.

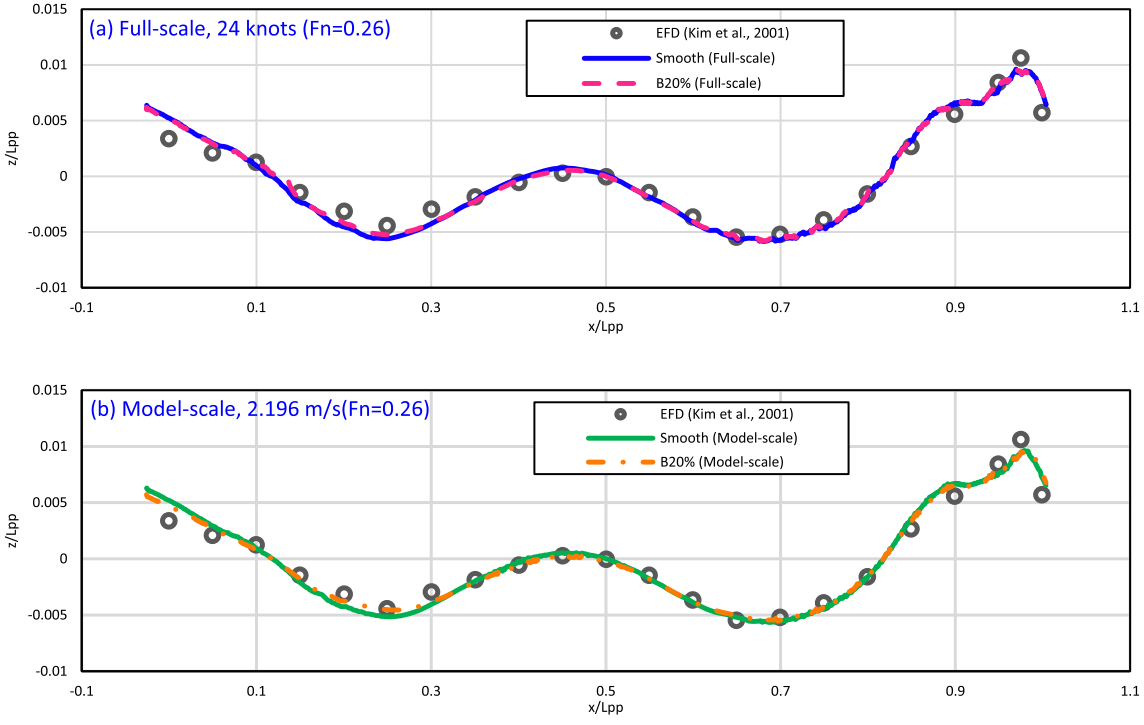

Fig. 12. Wave profile along the hull for smooth and fouled (B20%) cases, (a) full-scale, (b) model-scale.

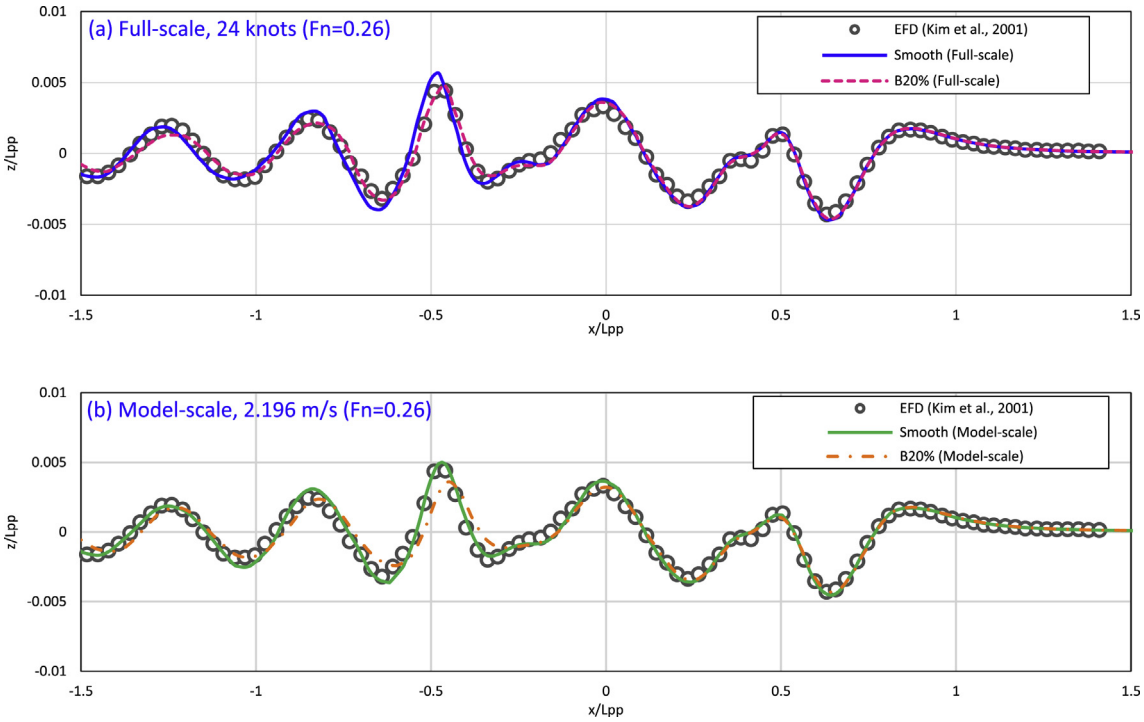

Fig. 13. Wave profile along a line with constant $y = 0.1509L_{pp}$ for smooth and fouled (B20%) cases, (a) full-scale, (b) model-scale.

fouling rate observed in Fig. 10.

3.5. Pressure distribution

Fig. 14 shows the pressure distribution along the KCS hull in the smooth and fouled (B20%) surface condition. It is clear from the figure that the surface roughness reduces the pressure recovery at the stern significantly, which increases the viscous pressure resistance, C_{VP} as observed from the previous section. It has been also observed that the surface roughness increases the pressure at the fore part of the rudder, which is believed due to the reduced flow velocity after the stern that can be seen in the following subsection. It is also notable that the pressure distributions of different surface conditions were similar from the bow to the middle of the ship. This finding denotes that the pressure distribution is not significantly affected by the surface roughness unless an adverse pressure gradient occurs, and hence it supports the assumption that the residuary resistance of the flat plates, which has zero pressure gradient, is not affected by the surface roughness (Schultz, 2007; Demirel et al., 2017a).

Fig. 15 illustrates the pressure contours at $y = 0.006L_{pp}$, downstream to the KCS in the smooth and fouled case (B20%) surface condition. It can be seen from the figure that the surface roughness decreases the magnitude of the pressure downstream to the hull. The significantly decreased pressure below the free surface behind the hull is in accordance with the reduce wave elevation after the stern in rough case as observed in Fig. 13.

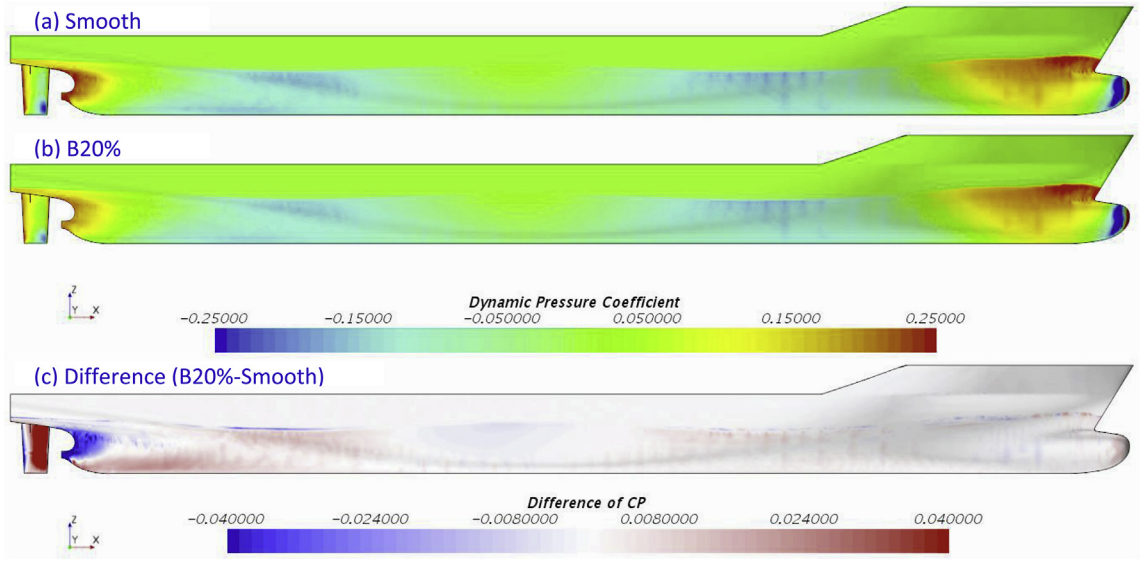

Fig. 14. Pressure distribution on the KCS hull, (a) smooth case, (b) fouled case (B20%), (c) difference (rough-smooth).

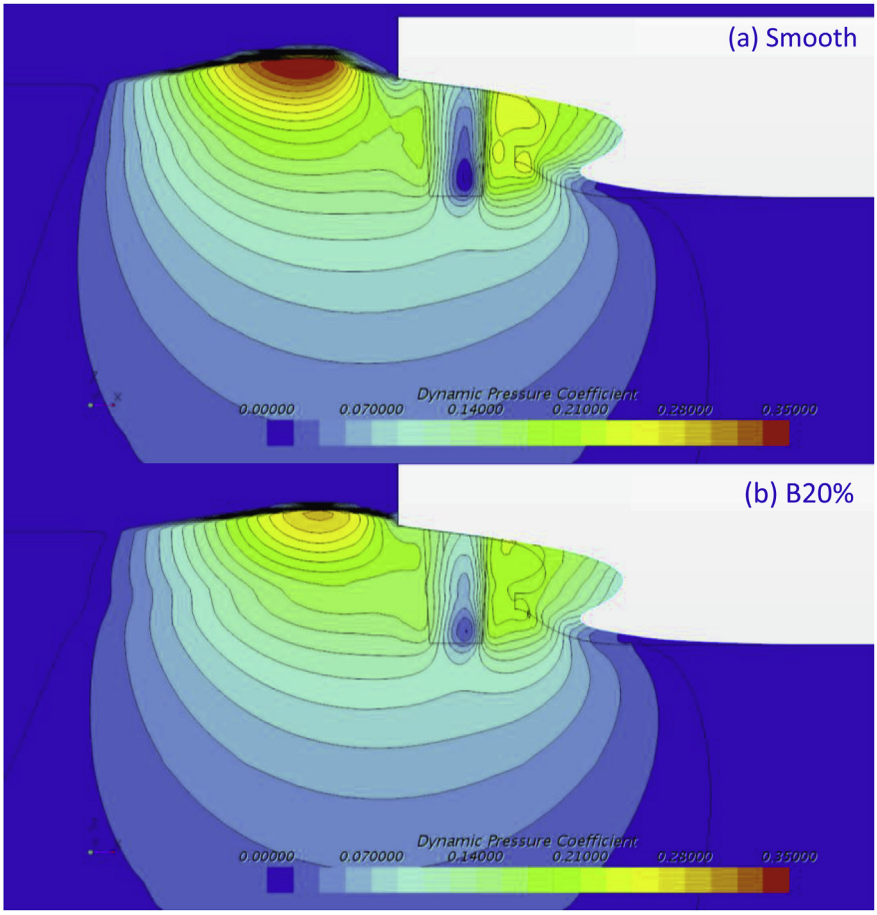

Fig. 15. Pressure distribution on the plane with constant $y = 0.006L_{pp}$, (a) smooth case, (b) fouled case, at 24 knots.

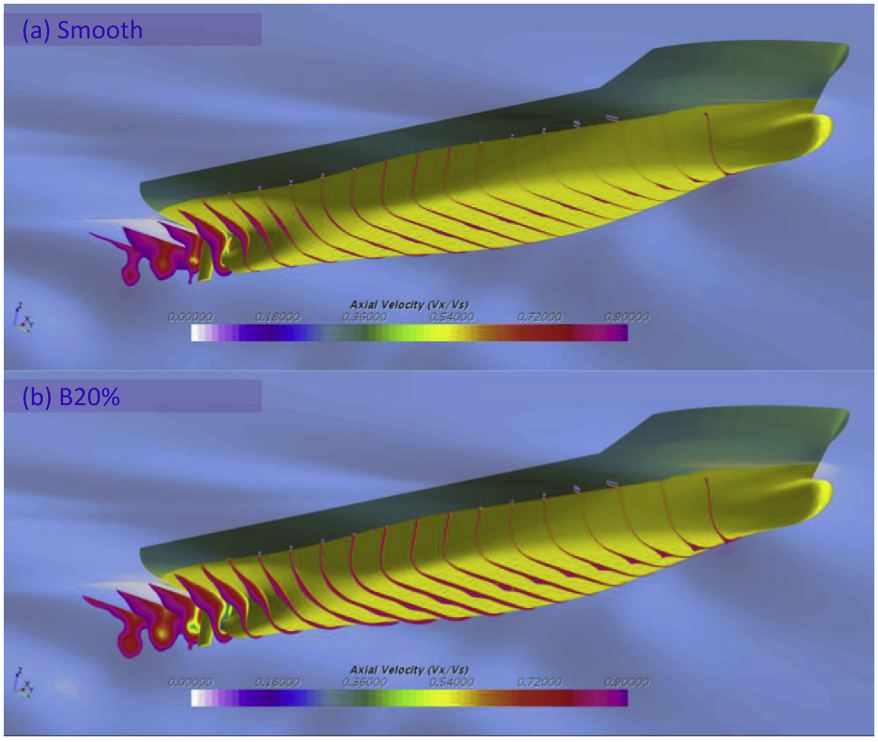

Fig. 16. Boundary layer represented by slices limited to axial velocity ($V_x/V_s = 0.9$), (a) smooth case, (b) fouled case.

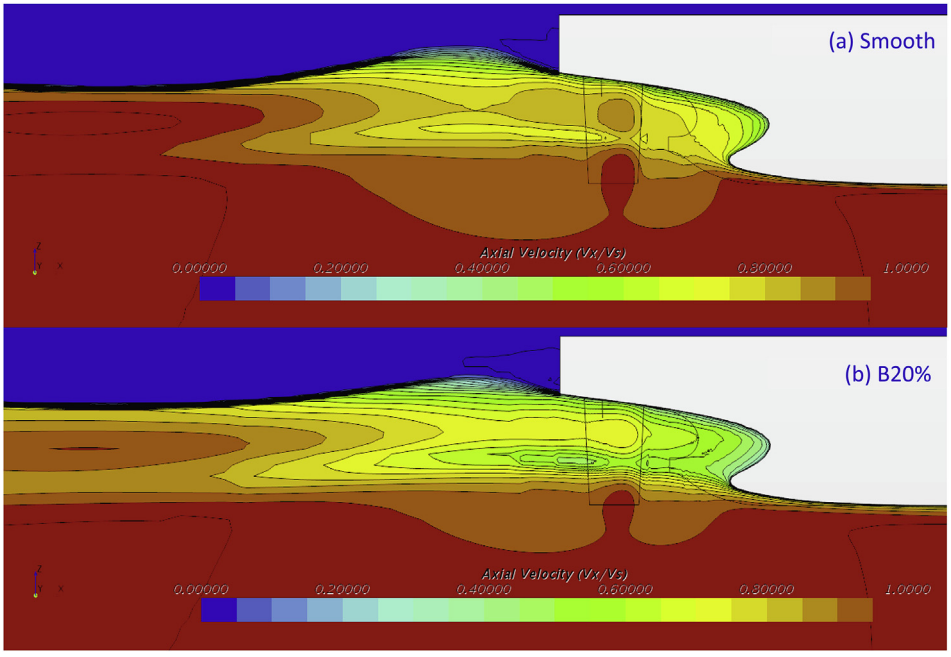

Fig. 17. Contours of mean axial velocity (V_x/V_s) at $y = 0.006L_{pp}$, (a) smooth case, (b) fouled case, at 24 knots.

3.6. Velocity distribution

Fig. 16 illustrates the boundary layer represented by the slices of axial velocity contours limited to $V_x/V_{ship} = 0.9$ for smooth and rough cases. It can be seen that the surface roughness results in the increased boundary layer thickness along the hull, and thus increase in the skin friction. This finding is consistent with the experimental and computational data of other researchers (e.g. Schultz and Flack, 2005, 2007; Flack et al., 2005; Flack et al., 2007; Schultz, 2000; Demirel et al., 2017b).

Fig. 17 compares the mean axial velocity contours around the stern of KCS for both smooth and rough cases at 24 knots. The mean axial velocity was non-dimensionalized by dividing the velocity by the advance velocity of the ship. As visually evident from the figure, the surface roughness decelerates the flow velocity around the ship stern and hence enlarges the wake field. It is believed that this enlarged wake region interacts with the pressure distribution at the stern and brings an increase in the viscous pressure resistance. Another notable point is that the surface roughness decreases the velocity below the free surface behind the hull, and hence it is likely seen that this deceleration of the water particles causes the reduced wave elevation after the stern in rough cases as observed in Fig. 13.

The wake (velocity) contour plots at a plane with constant $x = 0.0175L_{pp}$ at 24 knots are shown in Fig. 18 for the smooth and rough hull surfaces on the port and starboard half, respectively. It is clearly seen that the wake contours are strongly affected by the surface roughness. The rough case, B20%, has slowed down the wake velocities and hence enlarged the wake region due to the surface roughness. The decelerated flow around the hull can affect not only the ship resistance but also the propulsion performance of the ship as it affects the wake fraction at the propeller section.

3.7. Nominal wake

The analysis of the wake flow velocity at the stern region indicated that the surface roughness increases the wake flow which can be best represented by the classical nominal wake fraction parameter. Fig. 19 compares the distribution of the local wake fraction, $w_x' = 1 - V_x/V_{ship}$, and the transverse velocity vector, V_{xy}, at the propeller plane $x = 0.0175L_{pp}$ at 24knots. The inner and outer circles denote the hub diameter, D_H, and the propeller diameter, D_P, respectively. As shown in the figure, it is evident that the surface roughness of the hull increases the local wake fraction significantly. It was also observed that the surface roughness affects the direction and magnitude of the transverse flow at the propeller section.

Table 9 compares the mean nominal wake fraction, w_n, of the KCS in different surface conditions. The mean nominal wake fraction, w_n, was calculated by integrating the local wake fraction, w_x', over the propeller

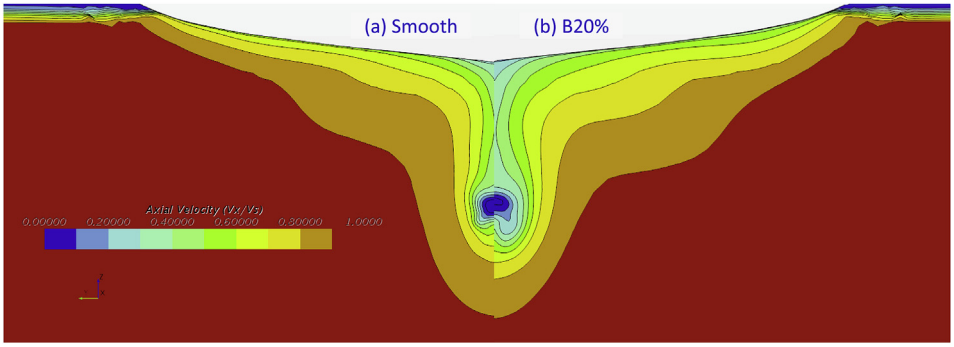

Fig. 18. Contours of mean axial velocity (V_x/V_s) at $x = 0.0175L_{pp}$, (a) smooth case, (b) fouled case, at 24 knots.

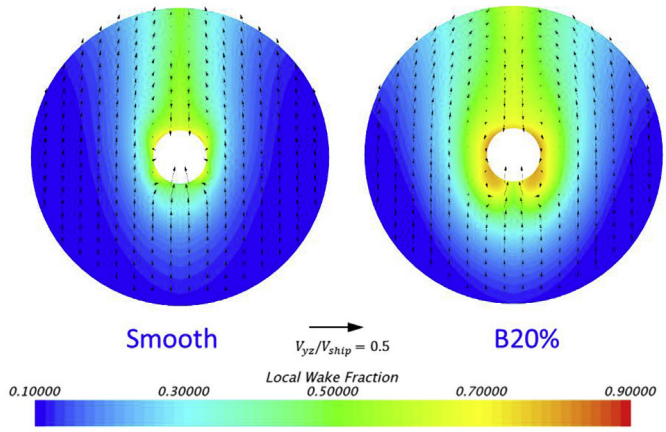

Fig. 19. Nominal wake distribution, w_x', and transvers velocity vector, V_{xy}, at the propeller plane in smooth and fouled cases, at 24 knots.

Table 9
Comparison of the mean nominal wake fraction computed from the simulations.

Surface condition	k_G (μm)	24 knots		19 knots	
		w_n	Δw_n	w_n	Δw_n
Smooth	0	0.1962	0%	0.2015	0%
S 10%	24	0.2350	20%	0.2265	12%
S 20%	63	0.2390	22%	0.2419	20%
M 10%	84	0.2444	25%	0.2474	23%
S 40%	149	0.2565	31%	0.2595	29%
M 20%	165	0.2588	32%	0.2619	30%
B 10%	174	0.2601	33%	0.2632	31%
S 50%	194	0.2627	34%	0.2659	32%
M 40%	388	0.2811	43%	0.2842	41%
M 50%	460	0.2862	46%	0.2892	44%
B 20%	489	0.2880	47%	0.2910	44%

disc. As indicated in the table, the increase in mean nominal wake fraction due to the barnacle fouling can be up to 47% and 44% at 24 knots and 19knots respectively. From this result, one may expect that the increase in wake fraction may compensate the negative effect of hull fouling in the resistance of the ship by increasing the hull efficiency, η_H. However, the decelerated inflow at the propeller section also affect the propeller efficiency, η_P, by altering the propeller advance coefficient, J. Therefore, in order to confirm the roughness effect on ship propulsion performance, a future work is needed using CFD simulations in self-propulsion conditions.

4. Concluding remarks

CFD models for the prediction of the effect of barnacle fouling on ship hydrodynamics have been proposed. To represent the surface roughness of barnacle fouling in the simulation, the roughness function of barnacles obtained by Demirel et al. (2017a) was adopted and embedded into the wall-function of the CFD software so that the surface boundary condition of the hull can represent the barnacle fouling.

For the validation of the modified wall-function approach, model-scale flat plate simulations representing different levels of barnacle fouling were modelled using the proposed approach. The simulation results showed excellent agreement with the experimental results of Demirel et al. (2017a).

A verification study was also conducted to assess the numerical uncertainties of the proposed CFD models and to determine sufficient grid-spacings and time steps. Spatial and temporal convergence studies were performed using the Grid Convergence Index (GCI) method.

Fully nonlinear unsteady RANS simulations of the full-scale flat plate representation of the KCS hull and the 3D representation of the same hull with rudder were performed to predict the effect of barnacle fouling on the resistance of this ship. The resulting frictional resistance coefficients were compared with each other, and also compared with the frictional resistance calculated by boundary layer similarity law scaling analysis and they all showed very good agreement in trends and magnitudes. It was observed that up to 93% and 88% of the frictional resistance increase at the design speed and the slow streaming speed can be experienced due to the barnacle fouling.

An interesting finding is that the residuary resistance values of the full-scale KCS show decreasing trend with increasing fouling rate at 24 knots whereas they show an opposite trend at 19 knots. The residuary resistance coefficients were separated into the viscous pressure resistance and wave making resistance coefficients, and it was observed that the wave making resistance decreases with increasing surface roughness while the viscous pressure resistance increases with the increasing fouling rate for both speeds. Therefore, it can be concluded that the residuary resistance can increase or decrease depending on the dominance of the wave making resistance and the viscous pressure resistance.

Another interesting finding is that the form factor of the ship also decreases as the surface roughness increases. This finding reveals that the increase in the viscous pressure resistance due to the surface roughness is not proportional to the increase in the frictional resistance, which disagrees with the assumptions of Lewis (1988) and Demirel et al. (2017b).

The roughness effect on the wave profile of the KCS was also examined by comparing those of smooth and rough simulation. As expected from the behaviour of the wave-making resistance coefficient, it has been found that the surface roughness results in smaller wave amplitude in the wake region.

By comparing the pressure distributions along the KCS hull in smooth and rough cases, it was found that the surface roughness reduces the pressure recovery at the stern, which results in increased viscous pressure resistance. It is notable that the pressure distributions were observed to be similar from the bow to the middle of the hull. This finding shows that the surface roughness does not affect the residuary resistance unless an adverse pressure gradient occurs, which supports the assumptions made by Schultz (2007) and Demirel et al. (2017a).

The effect of surface roughness on velocity distribution around the hull has also been explored. And it was observed that the surface roughness increases boundary layer thickness and enlarges wake region.

Another important finding from this study is that the stern wake of the ship is significantly affected by the surface roughness. It was found that up to 47% increase in nominal wake fraction can occur due to the hull fouling, which is likely to affect the propulsion performance of the ship.

This study has provided several important findings such as the roughness effect on the ship resistance, wave profile, pressure distribution along the hull, and the ship stern wake. Especially a notable increase in the nominal wake friction due to the surface roughness was observed. Therefore, future pieces of work may be the investigation of the roughness effect on ship propulsion performance.

Acknowledgements

It should be noted that the results were obtained using the ARCHIE-WeSt High Performance Computer (www.archie-west.ac.uk) based at the University of Strathclyde.

Appendix A. Supplementary data

Supplementary data to this article can be found online at https://doi.org/10.1016/j.oceaneng.2019.01.056.

References

Andrewartha, J., Perkins, K., Sargison, J., Osborn, J., Walker, G., Henderson, A., Hallegraeff, G., 2010. Drag force and surface roughness measurements on freshwater biofouled surfaces. Biofouling 26, 487–496.

Benson, J., Ebert, J., Beery, T., 1938. Investigation in the NACA Tank Fo the Effect of Immersion in Salt Water on the Resistance of Plates Coated with Different Shipbottom Paints. (Retrieved from).

Candries, M., Atlar, M., 2005. Experimental investigation of the turbulent boundary layer of surfaces coated with marine antifoulings. Journal of fluids engineering-transactions of the ASME 127 (2), 219–232.

Candries, M., Atlar, M., Mesbahi, E., Pazouki, K., 2003. The Measurement of the Drag Characteristics of Tin-free Self-Polishing Co-polymers and Fouling Release Coatings Using a Rotor Apparatus, vol. 19 (Suppl).

Castro, A.M., Carrica, P.M., Stern, F., 2011. Full scale self-propulsion computations using discretized propeller for the KRISO container ship KCS. Comput. Fluids 51 (1), 35–47. https://doi.org/10.1016/j.compfluid.2011.07.005.

CD-Adapco, 2017. STAR-CCM+ User Guide, version 12.06.

Celik, I.B., Ghia, U., Roache, P.J., Freitas, C.J., Coleman, H., Raad, P.E., 2008. Procedure for estimation and reporting of uncertainty due to discretization in CFD applications. J. Fluids Eng. 130 (7). https://doi.org/10.1115/1.2960953. 078001–078001-078004.

Clauser, F.H., 1954. Turbulent boundary layers in adverse pressure gradients. J. Aeronaut. Sci. 21 (2), 91–108. https://doi.org/10.2514/8.2938.

Date, J.C., Turnock, S.R., 1999. A Study into the Techniques Needed to Accrately Predict Skin Friction Using RANS Solvers with Validation against Froude's Histrical Flat Plate Experimental Data. (Retrieved from Southampton, UK).

Demirel, Y.K., 2015. Modelling the Roughness Effects of Marine Coatings and Biofouling on Ship Frictional Resistance. (PhD). University of Strathclyde, Glasgow.

Demirel, Y.K., Khorasanchi, M., Turan, O., Incecik, A., Schultz, M.P., 2014. A CFD model for the frictional resistance prediction of antifouling coatings. Ocean. Eng. 89, 21–31. https://doi.org/10.1016/j.oceaneng.2014.07.017.

Demirel, Y.K., Turan, O., Incecik, A., 2017b. Predicting the effect of biofouling on ship resistance using CFD. Appl. Ocean Res. 62, 100–118. https://doi.org/10.1016/j.apor.2016.12.003.

Demirel, Y.K., Uzun, D., Zhang, Y., Fang, H.-C., Day, A.H., Turan, O., 2017a. Effect of barnacle fouling on ship resistance and powering. Biofouling 33 (10), 819–834. https://doi.org/10.1080/08927014.2017.1373279.

Eça, L., Hoekstra, M., 2011. Numerical aspects of including wall roughness effects in the SST k–ω eddy-viscosity turbulence model. Comput. Fluids 40 (1), 299–314. https://doi.org/10.1016/j.compfluid.2010.09.035.

Ferziger, J.H., Peric, M., 2002. Computational Methods for Fluid Dynamics. Springer-Verlag Berlin Heidelberg.

Flack, K.A., Schultz, M.P., Connelly, 2007. Examination of a critical roughness height for outer layer similarity. Physics o fFluids 19 (9).

Flack, K.A., Schultz, M.P., Shapiro, T.A., 2005. Experimental support for Townsend's Reynolds number similarity hypothesis on rough walls. Phys. Fluids 17 (3), 035102. https://doi.org/10.1063/1.1843135.

Franzini, J., 1997. Fluid Mechanics with Engineering Aplications, ninth ed.9 ed. McGraw-Hill, New York.

Froude, W., 1872. Experiments on the Surface-Friction Experienced by a Plane Moving through Water. In the Collected Papaers of William Froude. British Association for the Advancement of Science, vol. 1955 Institution of Naval Architects.

Froude, W., 1874. Report to the Lords Commissioners of the Admiralty on Experiments for the Determination of the Frictional Resistance of Water on a Surface, under Various Conditions. (Retrieved from Chelston Cross:).

Gowing, S., Chang, P., Dehn, C., Storms, S., 2018. Measurements of biofouling drag using a 2-D channel flow apparatus with models of bio-fouled panels. In: Paper Presented at the the 19TH INTERNATIONAL CONGRESS on MARINE CORROSION and FOULING, (Melbourne, Florida).

Granville, P.S., 1958. The frictional resistance and turbulent boundary layer of rough surfaces. J. Ship Res. 2 (3), 52–74.

Granville, P.S., 1978. Similarity-law Characterization Methods for Arbitrary Hydrodynamic Roughnesses. Retrieved from, Bethesda, MD.

Granville, P.S., 1982. Drag-characterization method for arbitrarily rough surfaces by means of rotating disks. J. Fluid Eng. 104 (3), 373–377. https://doi.org/10.1115/1.3241854.

Granville, P.S., 1987. Three indirect methods for the drag characterization of arbitrarily rough surfaces on flat plates. J. Ship Res. 31 (No.1), 8.

Grigson, C., 1992. Drag losses of new ships caused by hull finish. J. Ship Res. 36, 182–196.

Holm, E., Schultz, M., Haslbeck, E., Talbott, W., Field, A., 2004. Evaluation of hydrodynamic drag on experimental fouling-release surfaces, using rotating disks. Biofouling 20 (4–5), 219–226. https://doi.org/10.1080/08927010400011245.

IMO, 2014. Third IMO GHG Study 2014, Executive Summary and Final Report. Retrieved from Suffolk, UK.

ITTC, 2011b. ITTC - Recommended Procedures and Guidelines: Practical Guidelines for Ship CFD Application.

ITTC, 2011c. ITTC - Recommended Procedures and Guidelines: Resistance Test.

ITTC, 2011a. Specialist Committee on Surface Treatment - Final Report and Recommendations to the 26th ITTC.

Izaquirre-Alza, P., Perez-Rojas, L., Nunez-Basanez, J.F., 2010. Drag reduction through special paints coated on the hull. In: Paper Presented at the International Conference on Ship Drag Reduction SMOOTH-SHIPS, (Istanbul, Turkey).

Karlsson, R.I., 1978. The effect of irregular surface roughness on the frictional resistance of ships. In: Paper Presented at the International Symposium on Ship Viscous Resistance, Swedish State Ship-Building Experimental Tank, (Goteborg).

Kempf, G., 1937. On the effect of roughness on the resistance of ships. Trans INA 79, 109–119.

Kim, W.J., Van, S.H., Kim, D.H., 2001. Measurement of flows around modern commercial ship models. Exp. Fluid 31 (5), 567–578. https://doi.org/10.1007/s003480100332.

Lackenby, H., 1962. The thirty-fourth Thomas Lowe Gray Lecture: resistance of ships, with special reference to skin friction and hull surface condition. Proc. Inst. Mech. Eng. 176 (1), 981–1014. https://doi.org/10.1243/PIME_PROC_1962_176_077_02.

Larsson, L., Stern, F., Visonneau, M., 2013. CFD in ship hydrodynamics—results of the gothenburg 2010 workshop. In: Eça, L., Oñate, E., García-Espinosa, J., Kvamsdal, T., Bergan, P. (Eds.), MARINE 2011, IV International Conference on Computational Methods in Marine Engineering: Selected Papers. Springer Netherlands, Dordrecht, pp. 237–259.

Lewis, E.V., 1988. Principles Of Naval Architecture : Resistance, Propulsion And Vibration: 2 Jersey City. The Society of Naval Architects and Marine Engineers.

Lewkowicz, A., Das, D., 1986. Turbulent boundary layers on rough surface with and without a pliable overlayer: a simulation of marine fouling. Int. Shipbuild. Prog. 33, 174–186.

Loeb, G., Laster, D., Gracik, T., 1984. The influence of microbial fouling films on hydrodynamic drag of rotating discs. In: Costlow, J.D., Tipper, R.C. (Eds.), Marine Biodeterioration: an Interdisciplinary Study, pp. 88–94.

McEntee, W., 1915. Variation of frictional resistance of ships with condition of wetted surface. Trans. - Soc. Nav. Archit. Mar. Eng. 24, 37–42.

Menter, F.R., 1994. Two-equation eddy-viscosity turbulence models for engineering applications. AIAA J. 32 (8), 1598–1605.

Moody, L.F., 1944. Friction Factors for Pipe Flow. Friction Factors for Pipe Flwo, vol. 66. Transactions of the American Society of Mechanical Engineers, pp. 671–681.

Owen, D., Demirel, Y.K., Oguz, E., Tezdogan, T., Incecik, A., 2018. Investigating the effect of biofouling on propeller characteristics using CFD. Ocean. Eng. https://doi.org/10.1016/j.oceaneng.2018.01.087.

Patel, V.C., 1998. Perspective: flow at high Reynolds number and over rough surfaces—achilles heel of CFD. J. Fluid Eng. 120 (3), 434–444. https://doi.org/10.1115/1.2820682.

Raven, H.C., Ploeg, A. v. d., Starke, A.R., Eça, L., 2008. Towards a CFD-based prediction of ship performance - progress in predicting full-scale resistance and scale effects. In: Paper presented at the RINA MArine CFD Conference, London.

Richardson, L.F., 1910. The approximate arithmetical solution by finite differences of physical problems involving differential equations, with an application to the stresses in a masonry dam. Transcations of the Royal Society of London. Series A 210, 307–357.

Schultz, M.P., 2000. Turbulent boundary layers on surfaces covered with filamentous algae. J. Fluid Eng. 122 (2), 357–363. https://doi.org/10.1115/1.483265.

Schultz, M.P., 2004. Frictional resistance of antifouling coating systems. J. Fluid Eng. 126 (6), 1039–1047. https://doi.org/10.1115/1.1845552.

Schultz, M.P., 2007. Effects of coating roughness and biofouling on ship resistance and powering. Biofouling 23 (5), 331–341. https://doi.org/10.1080/08927010701461974.

Schultz, M.P., Flack, K.A., 2005. Outer layer similarity in fully rough turbulent boundary layers. Exp. Fluid 38 (3), 328–340. https://doi.org/10.1007/s00348-004-0903-2.

Schultz, M.P., Flack, K.A., 2007. The rough-wall turbulent boundary layer from the hydraulically smooth to the fully rough regime. J. Fluid Mech. 580, 381–405. https://doi.org/10.1017/S0022112007005502.

Schultz, M.P., Myers, A., 2003. Comparison of three roughness function determination methods. Exp. Fluid 35 (4), 372–379. https://doi.org/10.1007/s00348-003-0686-x.

Schultz, M.P., Swain, G.W., 1999. The effect of biofilms on turbulent boundary layers. J. Fluid Eng. 121 (1), 44–51. https://doi.org/10.1115/1.2822009.

Schultz, M.P., Swain, G.W., 2000. The influence of biofilms on skin friction drag. Biofouling 15 (1–3), 129–139. https://doi.org/10.1080/08927010009386304.

Schultz, M.P., Walker, J.M., Steppe, C.N., Flack, K.A., 2015. Impact of diatomaceous biofilms on the frictional drag of fouling-release coatings. Biofouling 31 (9–10), 759–773. https://doi.org/10.1080/08927014.2015.1108407.

Shapiro, T.A., 2004. The Effect of Surface Roughness on Hydrodynamic Drag and Turbulence. (Retrieved from).

Terziev, M., Tezdogan, T., Oguz, E., Gourlay, T., Demirel, Y.K., Incecik, A., 2018. Numerical investigation of the behaviour and performance of ships advancing through restricted shallow waters. J. Fluid Struct. 76, 185–215. https://doi.org/10.1016/j.jfluidstructs.2017.10.003.

Tezdogan, T., Demirel, Y.K., Kellett, P., Khorasanchi, M., Incecik, A., Turan, O., 2015. Full-scale unsteady RANS CFD simulations of ship behaviour and performance in head seas due to slow steaming. Ocean. Eng. 97, 186–206. https://doi.org/10.1016/j.oceaneng.2015.01.011.

Townsin, R.L., 2003. The ship hull fouling penalty. Biofouling 19 (supp. 1), 9–15. https://doi.org/10.1080/0892701031000088535.

UNCTAD, 2017. Review of Maritime Transport. Retrieved from Geneva, Switzerland.

Watanabe, S., Nagmatsu, N., Yokoo, K., Kawakami, Y., 1969. The augmentation in frictional resistance due to slime. J. Kansai Soc. Nav. Arc. 131 (45–51).

White, F.M., 2011. Fluid Mechanics. McGraw Hill.

Womack, K.M., Schultz, M.P., Meneveau, C., 2018. Effect of Barnacle Density on Hydrodynamic Drag. In: Paper Presented at the the 19th international congress on marine corrosion and fouling, (Melbourne, Florida).